

# Density functional study of two-dimensional $^4\text{He}$ clusters

J. Mur-Petit

*Departament d'Estructura i Constituents de la Matèria, Universitat de Barcelona, Avinguda Diagonal, 647, E-08028 Barcelona, Spain*

A. Sarsa

*Departamento de Física, Campus de Rabanales, Universidad de Córdoba, E-14071 Córdoba, Spain*

J. Navarro

*IFIC, CSIC-Universitat de València, Apartado 20285, E-46071 València, Spain*

A. Polls

*Departament d'Estructura i Constituents de la Matèria, Universitat de Barcelona, Avinguda Diagonal 647, E-08028 Barcelona, Spain*

(Received 24 May 2005; published 20 September 2005)

Binding energies and density profiles of two-dimensional systems of liquid  $^4\text{He}$  with different geometries are studied by means of a zero-range density functional adjusted to reproduce the line tension obtained in a previous diffusion Monte Carlo calculation ( $\lambda_{\text{DMC}}=0.121 \text{ K}/\text{\AA}$ ). It is shown that this density functional provides accurate results for the binding energy of large clusters with a reasonable computational effort.

DOI: [10.1103/PhysRevB.72.104513](https://doi.org/10.1103/PhysRevB.72.104513)

PACS number(s): 67.70.+n, 36.40.-c, 68.03.Cd, 31.15.Ew

## I. INTRODUCTION

Quantum liquids in restricted geometries have attracted a lot of attention in recent years.<sup>1</sup> One interesting feature of these systems is that their internal structure is more accessible than in bulk liquids due to the restricted motion of the atoms in the confining potential. Among these systems the study of two-dimensional systems has received particular attention. An example of such a system is liquid helium adsorbed to a more-or-less attractive flat surface. This kind of system was observed for the first time by M. Bretz *et al.*<sup>2</sup> in 1973, when they reported the observation of adsorbed  $^4\text{He}$  onto the basal plane of graphite. In the last few years, adsorption properties of helium on many different substrates (carbon, alkali and alkaline-earth flat surfaces, carbon nanotubes, aerogels) have become a fruitful topic of research.

Theoretical microscopic studies with realistic atom-atom interactions, such as that of Clements *et al.*,<sup>3</sup> have shown that films with low surface coverages, where all atoms cover the surface with a thickness corresponding to a single atom, can be reasonably approximated by a two-dimensional (2D) model. In connection with these systems, an interesting question naturally arises as to how physics depends on the dimensionality of the space.

The homogeneous 2D liquid has been studied using different theoretical methods, such as molecular dynamics<sup>4</sup> and quantum Monte Carlo simulations, either Green's function<sup>5</sup> or diffusion<sup>6</sup> techniques.

Recently, two-dimensional clusters of liquid  $^4\text{He}$  have been studied using a shadow variational wave function,<sup>7</sup> and also by the diffusion Monte Carlo (DMC) method.<sup>8</sup> In these two references, the binding energies of the 2D clusters were fitted by means of a mass formula and a line tension of  $\lambda=0.121 \text{ K}/\text{\AA}$  was reported in Ref. 8. However, due to computational limitations, the number of atoms in the clusters

was limited to  $N\sim 100$ . In addition, the density profiles of the clusters, especially for coordinates close to the origin, are usually obtained in the Monte Carlo method with poor statistics. Therefore, it seems appropriate to build a density functional suitable to be used in 2D, using the same procedure which has already been successfully used to study three-dimensional (3D)  $^4\text{He}$  clusters.<sup>9,10,12</sup>

Density functionals are based on the well-known Hohenberg-Kohn theorem<sup>11</sup> that asserts that the ground-state energy per particle of a many-body system can be written as a functional of the density. Once the functional is available, its minimization brings us to a Euler-Lagrange equation<sup>12</sup> for the density profile  $\rho(\mathbf{r})$ , which allows us to calculate the properties of clusters. Note that the results obtained with the density functional will be more reliable for larger clusters, as it has been constructed to reproduce properties of the homogeneous and semi-infinite media.

The density functional we use is the simplest version of the zero-range functional intensively used in 3D.<sup>13</sup> Its parameters have been adjusted so as to reproduce some properties of the ground state of the homogeneous system as obtained in DMC calculations,<sup>6</sup> as well as the line tension extracted from the mass formula of Ref. 8. This procedure is discussed in Sec. II, together with the results for the slabs. Section III is devoted to the study of finite droplets, with a special emphasis on those with a large number of atoms. Finally, in Sec. IV, the main conclusions are summarized.

## II. SEMI-INFINITE SYSTEM AND SLABS

Density functionals to investigate surface properties of superfluid  $^4\text{He}$  were developed during the 1970s.<sup>14</sup> At zero temperature and in the absence of currents, the order param-

eter of a bosonic system is nothing but the square root of the one-body density  $\rho(\mathbf{r})$ , so it is natural to think of the energy of the system as a functional of the helium density. Stringari<sup>13</sup> proposed a zero-range density functional for non-homogeneous three-dimensional <sup>4</sup>He systems of the form

$$E[\rho] = \int d\mathbf{r} \left\{ \frac{\hbar^2}{2m} \frac{|\nabla\rho|^2}{4\rho} + b\rho^2 + c\rho^{2+\gamma} + d|\nabla\rho|^2 \right\}, \quad (1)$$

which was used to study <sup>4</sup>He surface properties<sup>15</sup> and clusters.<sup>9</sup>

For the two-dimensional systems, we will use the same functional form. However, the parameters  $b$ ,  $c$ ,  $\gamma$  characterizing the functional for homogeneous systems have to be recalculated by requiring that the functional reproduces some known properties of the two-dimensional <sup>4</sup>He system, such as the ground-state energy per particle ( $e_0 = -0.89706$  K), saturation density ( $\rho_0 = 0.04344 \text{ \AA}^{-2}$ ), and the compressibility (or the velocity of sound,  $s = 92.8$  m/s), which were derived in the framework of the diffusion Monte Carlo method.<sup>6</sup> In addition, the parameter  $d$  is obtained by demanding that the line tension of the semi-infinite system equals that obtained from DMC calculations for 2D clusters,  $\lambda = 0.121 \text{ K/\AA}$ .<sup>8</sup> The energy per particle for the homogeneous system provided by this functional reproduces very well the equation of state obtained from DMC calculations in a wide range of densities.<sup>6</sup> Therefore, as a first step we need to study the semi-infinite system. In principle, one should solve a Euler-Lagrange equation for the density profile  $\rho(\mathbf{r})$  which results from minimizing the energy functional of Eq. (1) after introducing the Lagrange multiplier ( $\mu$ ), which is identified with the chemical potential,

$$\frac{\hbar^2}{8m} \left[ -\frac{2\nabla^2\rho}{\rho} + \frac{|\nabla\rho|^2}{\rho^2} \right] + 2b\rho + (2+\gamma)c\rho^{1+\gamma} - 2d\nabla^2\rho = \mu. \quad (2)$$

One should also impose the boundary condition,  $\rho(x \rightarrow -\infty) = \rho_0$ . However, for the particular case of a zero-range functional, the line tension of the semi-infinite system can be evaluated in a closed form, without solving for the density profile

$$\lambda = 2 \int_0^{\rho_0} d\rho \left[ \left( \frac{\hbar^2}{8m} + \rho d \right) (b\rho + c\rho^{1+\gamma} - \mu) \right]^{1/2}. \quad (3)$$

Then, imposing  $\lambda = 0.121 \text{ K/\AA}$  (Ref. 8), one gets an implicit equation  $\lambda = \lambda(d)$  which can be solved numerically, thus fixing the last parameter of the functional. The parameters for the two-dimensional zero-range functional are listed in Table I.

Once the functional is defined, one can study any two-dimensional <sup>4</sup>He system. The first systems we have considered are two-dimensional slabs with varying central density  $\rho_c = \rho(0)$ . A systematic study of three-dimensional <sup>4</sup>He slabs

TABLE I. Parameters of the two-dimensional zero-range functional.

$b$ (K $\text{\AA}^2$ )	$c$ (K $\text{\AA}^{2(1+\gamma)}$ )	$\gamma$	$d$ (K $\text{\AA}^4$ )
-26.35	$4.88 \times 10^5$	3.62	359

with different density functionals has been presented in Ref. 16. The Euler equation for the slabs is the same as for the semi-infinite system [Eq. (2)]. The changes in the solution of the equation originate from the different geometry and boundary conditions which define the slab. Translational symmetry implies that the density depends only on the coordinate perpendicular to the slab surface, which we call  $x$ . Then,  $\nabla\rho = \rho'(x)$  and  $\nabla^2\rho = \rho''(x)$ , where the prime denotes derivative with respect to  $x$ . In this way, the Euler equation [Eq. (2)] can be expressed in a more convenient form, in which now  $\rho$  depends only on  $x$ ,

$$\frac{\hbar^2}{8m} \left( \frac{(\rho')^2}{\rho^2} - \frac{2\rho''}{\rho} \right) - 2d\rho'' + 2b\rho + (\gamma+2)c\rho^{1+\gamma} = \mu. \quad (4)$$

In the next step, one eliminates the second derivative of Eq. (4) by multiplying both sides of the equation by  $\rho'$  and integrating with respect to  $x$ , from the origin to a given value of  $x$ ,

$$\left[ -\frac{\hbar^2}{8m} \frac{(\rho')^2}{\rho} - d(\rho')^2 + b\rho^2 + c\rho^{\gamma+2} \right]_0^x = \mu[\rho(x) - \rho(0)]. \quad (5)$$

Imposing  $\rho(\infty) = \rho'(\infty) = 0$ , and considering that the slab is symmetric respect to  $x=0$ , and therefore  $\rho'(0) = 0$ , one obtains the chemical potential as a function of the central density of the slab,

$$\mu = b\rho_c + c\rho_c^{\gamma+1}. \quad (6)$$

We remark that this chemical potential is constant along the profile.

Going back to Eq. (5), and using the fact that  $\rho'(0) = 0$ , one obtains

$$\rho' = \sqrt{\frac{\rho^2(b\rho + c\rho^{\gamma+1} - \mu)}{\hbar^2/8m + d\rho}}. \quad (7)$$

This expression for  $\rho'$  is then used to calculate the number of atoms per unit length along the  $y$  axis (parallel to the surface), i.e., the coverage, in a closed expression, in terms of  $\rho$ ,

$$\begin{aligned} \frac{N}{L} &= 2 \int_0^\infty \rho(x) dx = 2 \int_0^{\rho(0)} \rho \frac{d\rho}{|\rho'|} \\ &= 2 \int_0^{\rho(0)} d\rho \sqrt{\frac{\hbar^2/8m + d\rho}{b\rho + c\rho^{1+\gamma} - \mu}}. \end{aligned} \quad (8)$$

This integral has a singularity when  $\rho \rightarrow \rho_c$ , which can be avoided by performing an integration by parts. The final expression, free of numerical problems, reads

$$\frac{N}{L} = -\frac{4}{b} \sqrt{-\frac{\hbar^2}{8m}\mu - 4} \int_0^{\rho(0)} d\rho \frac{(b\rho + c\rho^{1+\gamma} - \mu)^{1/2} \left[ \frac{d}{2} [b + c(1+\gamma)\rho^\gamma] - \left( \frac{\hbar^2}{8m} + d\rho \right) c\gamma(1+\gamma)\rho^{\gamma-1} \right]}{[b + c(1+\gamma)\rho^\gamma]^2 \left( \frac{\hbar^2}{8m} + d\rho \right)^{1/2}}.$$

Also useful is the energy per unit length,

$$\frac{E}{L} = 2 \int_0^\infty dx \left[ \frac{\hbar^2}{8m} \frac{(\rho')^2}{\rho} + b\rho^2 + c\rho^{2+\gamma} + d(\rho')^2 \right]. \quad (9)$$

Using the Euler equation [Eq. (7)] and the previous definition of the coverage, one can finally express the energy per particle  $e = E/N$  in terms of the inverse of the coverage,  $\tilde{x} = L/N$ ,

$$e(\tilde{x}) = \mu(\tilde{x}) + 4\tilde{x} \int_0^{\rho(0)} d\rho \sqrt{\left( \frac{\hbar^2}{8m} + d\rho \right) [b\rho + c\rho^{1+\gamma} - \mu(\tilde{x})]}. \quad (10)$$

Therefore, given  $\rho(0) \in [0, \rho_0]$ , and using the previous expressions, one can calculate the chemical potential, the coverage, and the energy per particle.

The energy per particle and the chemical potential as a function of the inverse of the coverage  $\tilde{x}$  are reported in Fig. 1. In the limit  $\tilde{x} \rightarrow 0$ , one recovers the binding energy at  $\rho_0$  of the uniform system, which in turn coincides with the chemical potential. The energy per particle has a very clean linear behavior at the origin, as illustrated by the solid straight line which provides a very good description of the energy per particle up to  $\tilde{x} \sim 1.5$  Å. The slope of this line can be analytically derived and turns out to be twice the linear tension. As a consequence of the linear tension, the binding energy per particle of the slab decreases with the inverse of the coverage. Actually, the derivation of the linear behavior of the binding energy per particle can be obtained starting from Eq. (10), which defines the energy per particle as a function of  $\tilde{x}$ , by performing an expansion around  $\tilde{x} = 0$ ,

$$e(\tilde{x}) = \mu_\infty + 2\sigma\tilde{x} + \dots \quad (11)$$

For values larger than  $\tilde{x} \sim 1.5$  Å the binding energy per particle starts to bend towards the  $\tilde{x}$  axis and becomes a convex function, which will slowly approach zero. The chemical potential is very flat at the origin, being determined by the central density of the slab. The ratio of the central density to the equilibrium density as a function of the inverse of the coverage is displayed in the lower panel of Fig. 1. In agreement with the chemical potential, the central density is very flat at small values of  $\tilde{x}$ . The central density of a slab can never go above the equilibrium density and it is always a decreasing function of  $\tilde{x}$ . The flatness of the central density and the chemical potential for small values of  $\tilde{x}$  indicate that the slab very slowly approaches the limit of the infinite system.

The density profiles of the slabs can be obtained from the following relation:

$$\int_{\rho(x)}^{\rho_c} d\rho \left[ \frac{\frac{\hbar^2}{8m}\rho + d}{b\rho^2 + c\rho^{2+\gamma} - \mu\rho} \right]^{1/2} = x, \quad (12)$$

valid for  $x \geq 0$ . Notice also the presence of a divergence when  $\rho \rightarrow \rho_c$  which can be again avoided by performing an integration by parts. The profiles calculated for various central densities are plotted in Fig. 2. The size of the slab increases with the central density. A measure of this size is given by the radius  $R$ , defined as the distance from the origin to the point where the density has fallen to half its central value. The radius of the slabs as a function of  $\tilde{x}$  is shown in the top panel of Fig. 3. As expected, the radius diverges in the limit  $\rho_c \rightarrow \rho_0$  and is a decreasing function of  $\tilde{x}$ . It also presents a very shallow minimum around  $\tilde{x} \sim 3.3$  Å. The profiles are also characterized by the thickness  $t$ , defined as the distance between the points where the density has decreased from 90% to 10% of its central value. The thickness as a function of  $\tilde{x}$  is reported in the lower part of Fig. 3. Up to

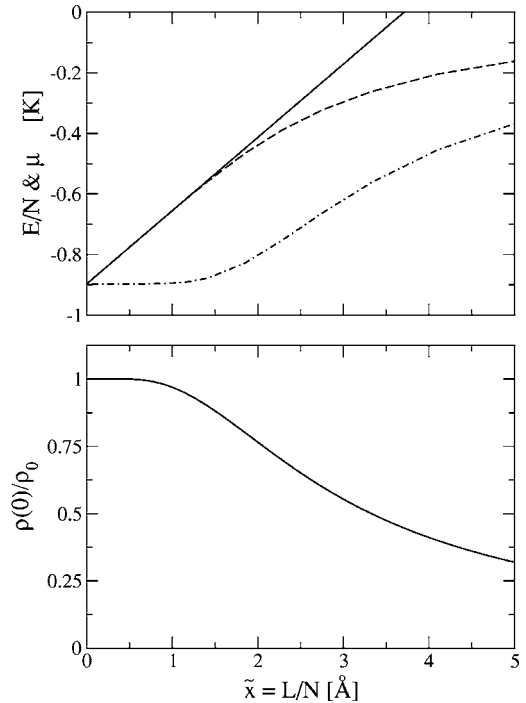


FIG. 1. (Top) Energy per particle (dashed line) and chemical potential (dot-dashed line) for  ${}^4\text{He}$  slabs as a function of the inverse of the coverage. The solid straight line corresponds to the asymptotic behavior of the energy per particle and its slope is determined by the linear tension of the semi-infinite system. (Bottom) Ratio between the central density and the bulk equilibrium density for  ${}^4\text{He}$  slabs as a function of the inverse of the coverage.

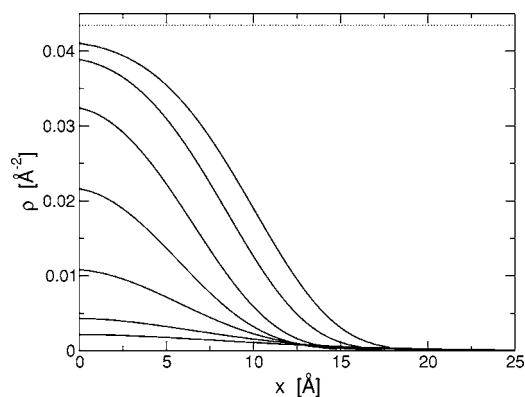


FIG. 2. Density profiles for  ${}^4\text{He}$  slabs with central densities  $\rho_c/\rho_0=0.05, 0.1, 0.25, 0.5, 0.75, 0.9, 0.95$ , where  $\rho_0$  is the equilibrium density of the bulk. The horizontal dotted line corresponds to the bulk density  $\rho_0$ .

$\tilde{x} \sim 1$ , the thickness is a flat function, indicating that the surface of the slab is very much the same, and is actually the radius of the slab that grows very fast and diverges when  $\tilde{x} \rightarrow 0$ . The thickness is very large for the smaller slabs; as each particle interacts with very few others, the system extends to very large distances. When the central density is increased ( $\tilde{x}$  decreases), the thickness decreases until it has a minimum at  $\tilde{x} \approx 2.75 \text{ \AA}$ , with  $t \approx 8.6 \text{ \AA}$ . Then, it increases again approaching a finite value corresponding to the semi-infinite medium,  $t \approx 11.03 \text{ \AA}$ .

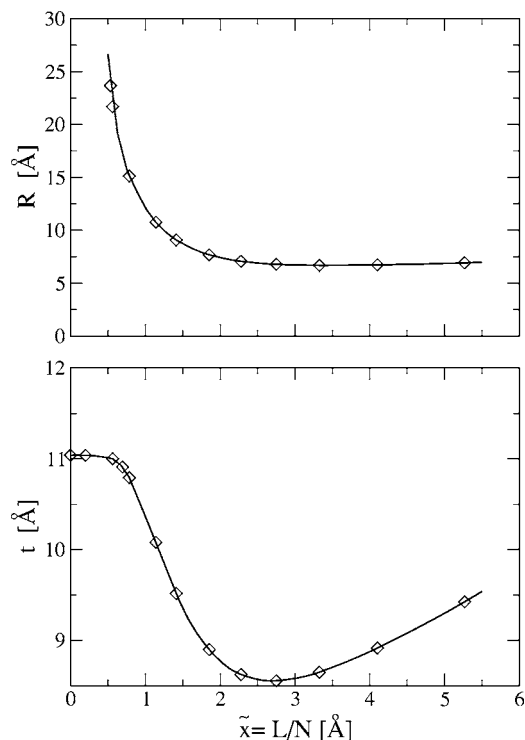


FIG. 3. Radius (top panel) and thickness (lower panel) of  ${}^4\text{He}$  slabs as a function of  $\tilde{x}$ . The symbols are the calculated data while the lines are cubic splines to guide the eye.

### III. DROPS AND LINE TENSION

As a next step, we consider finite systems and, in particular, drops of fixed numbers of atoms  $N$ . These were already studied by DMC techniques in Ref. 8. However, computational limitations allowed only the study of small values of  $N$ . Here, we will take advantage of the computational feasibility of the density functional calculations and will extend the analysis to much greater  $N$ . In this way it is possible to study the asymptotic behavior of several quantities which characterize the drops.

In this case, Eq. (2) for the profile can be rewritten in the form of a Schrödinger-like equation for  $\rho$ ,

$$\begin{aligned} \mathcal{H}\rho &\equiv -\frac{\hbar^2}{4m} \left[ \nabla^2 \rho - \frac{|\nabla \rho|^2}{2\rho^2} \right] + 2b\rho + (2 + \gamma)c\rho^{1+\gamma} - 2d\nabla^2 \rho \\ &= \mu\rho. \end{aligned} \quad (13)$$

As the number of atoms is a well defined  $N$ , one would need to be very careful in determining the central density  $\rho(0)$  so that the chemical potential adjusted exactly to  $N$ . However, it turns out that this equation is more efficiently solved by means of the steepest descent method.<sup>17</sup> An initial trial  $\rho(r)$  is projected onto the minimum of the functional by propagating it in imaginary time. In practice, one chooses a small time step  $\Delta t$  and iterates the equation

$$\rho(r, t) \approx \rho(r, t) - \Delta t \mathcal{H}\rho(r, t) \quad (14)$$

by normalizing  $\rho$  to the total number of atoms at each iteration. The time step that governs the rate of convergence should be taken appropriately small in such a way that Eq. (14) is a valid approximation. Convergence is reached when the chemical potential has a constant value independent of position.

The energy per particle (empty circles) and the chemical potential (full circles) of each drop are reported in Fig. 4 as a function of  $N^{-1/2}$ . Also shown are the DMC results (empty squares) and their quadratic fit reported in Ref. 8. The calculated energies of the droplets can be represented very accurately with a mass formula of the type

$$e(N) = \epsilon_b + \epsilon_l z + \epsilon_c z^2 + \dots, \quad (15)$$

with  $z = N^{-1/2}$ . The two first coefficients of this expansion are the bulk energy  $\epsilon_b$  and the line energy  $\epsilon_l$ , out of which the line tension  $\lambda$  is defined by  $2\pi r_0 \lambda = \epsilon_l$ . Here  $r_0$  is the unit radius, defined as the radius of a disk whose surface is equal to the inverse of the equilibrium density of the 2D bulk liquid, i.e.,  $\rho_0 \pi r_0^2 = 1$ . Finally,  $\epsilon_c$  can be related to the so-called curvature energy. Contrary to the DMC calculations where the largest droplet that we studied had 121 atoms, here we have considered droplets with up to 10 000 atoms. In this way we can accurately study the behavior of the energy per particle for small values of  $z$ . Doing a quadratic fit to the calculated energies per particle for  $N \geq 512$  and including also the bulk binding energy for  $z=0$ , one gets

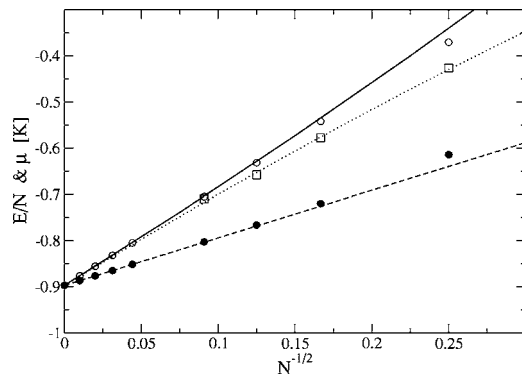


FIG. 4. Energy per particle (empty circles) and chemical potential (full circles) of  ${}^4\text{He}$  droplets as a function of  $N^{-1/2}$ . Also shown is a quadratic fit (see text) of the results with  $N > 516$  (solid line). The straight short-dashed line is obtained when the mass formula (with terms up to  $z^2$ ) is used to calculate the chemical potential. The empty squares are DMC results from Ref. 8 and the dotted line corresponds to the quadratic fit to these results reported in the same reference.

$$y = -0.897 + 2.0587z + 0.66466z^2, \quad (16)$$

which is plotted by a solid line in Fig. 4. One sees that  $\epsilon_b$  accurately reproduces the bulk energy per particle, which was used to fix the parameters of the functional. The value of  $\epsilon_f = 2.0587$  corresponds to a line tension  $\lambda = 0.121 \text{ K}/\text{\AA}$ , which is the same as the value of the line tension of the semi-infinite system, used to build the density functional. Note that this fit, even if it has been calculated for  $N \geq 512$ , is rather accurate down to  $N = 36$ . Obviously, one cannot expect a good agreement for  $N = 16$ . The linear behavior of the chemical potential as a function of  $z$  is easy to understand using the mass formula [Eq. (15)] and the thermodynamic definition of the chemical potential  $\mu = \partial E / \partial N$ , where  $E$  is the total energy of the droplet. Using this prescription, the slope of the chemical potential as a function of  $z$  results in  $\epsilon_f/2$ . A similar plot for the energy per particle in the three-dimensional case in terms of  $N^{-1/3}$  would provide a behavior of the chemical potential for large  $N$ , dominated also by a linear component with a slope at the origin given by  $2\epsilon_s/3$ , where  $\epsilon_s$  is the surface energy associated to three-dimensional clusters.<sup>9</sup>

Also interesting is the fact that the coefficient of  $z^2$  is positive. This sign corresponds to the expected loss of binding energy associated with the curvature of the contour of the cluster. This is in contrast to the value of  $\epsilon_c$  obtained by fitting DMC results, as was done in Ref. 8. However, in that case the number of particles in the clusters used to build the fit was much smaller, with  $N = 121$  the largest number of particles and going down to  $N = 8$  for the smallest one. In the present fit we have explicitly avoided the clusters with a small number of particles which can easily distort the results, and we have considered only the cases with  $N \geq 512$ .

The next things to analyze are the density profiles which are reported in Fig. 5 for different numbers of atoms. Contrary to the slabs, the central density of the droplets can be

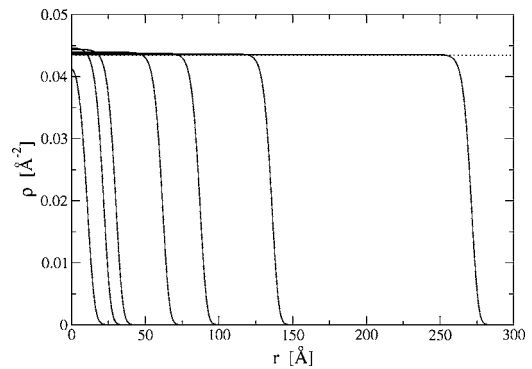


FIG. 5. Density profiles for  ${}^4\text{He}$  droplets for  $N = 16, 64, 121, 512, 1024, 2500,$  and  $10\,000$  atoms. The continuous lines are generalized Fermi profiles [Eq. (17)] fitted to the data (see Table II). The dotted horizontal line indicates the equilibrium density  $\rho_0$ .

higher than the saturation density, which is indicated in the figure by a horizontal line. The profiles are well adjusted by a function of the type

$$\rho(r) = \frac{\rho_f}{(1 + e^{(r-R)/c})^\nu}, \quad (17)$$

which has an associated central density  $\rho(0) = \rho_f / (1 + e^{-R/c})^\nu$ . The parameters defining the profiles for the different numbers of atoms are provided in Table II, together with the thickness and root-mean-square radius obtained from these fits.

The upper part of Fig. 6 reports the central density of the different droplets as a function of  $z$ . For large values of  $N$ , the central density is larger than the saturation density, i.e., the central part of the droplet is more compressed than the bulk system, which is sometimes referred to as a leptodermous behaviour.<sup>9</sup> Of course for  $N \rightarrow \infty$  the central density tends to the equilibrium density of the homogeneous liquid. First, the central density grows almost linearly with  $z$ , reaches a maximum for  $N \sim 60$ , which would correspond to the most compressed droplet, and then decreases. Finally for  $N \leq 25$  the central region of the droplets becomes less compressed than the bulk system.

TABLE II. Parameters of a generalized Fermi-profile fit [Eq. (17)] to the density profiles obtained with the zero-range density functional. All lengths are in  $\text{\AA}$  and  $\rho_f$  is in  $\text{\AA}^{-2}$ . The parameter  $\nu$  is adimensional.

$N$	$\rho_f$	$R$	$c$	$\nu$	$t$	$\langle r^2 \rangle^{1/2}$
16	0.04321	13.2718	3.22067	2.13417	11.746	9.66
36	0.04494	19.1852	3.22054	2.37516	11.548	12.793
64	0.04974	24.6826	3.16845	2.37072	11.364	16.28
121	0.04441	32.8314	3.12302	2.33636	11.226	21.72
512	0.04392	64.4245	3.08867	2.32368	11.112	43.533
1024	0.04378	89.8497	3.08584	2.32997	11.097	61.342
2500	0.04366	138.628	3.08552	2.33826	11.090	95.678
10000	0.04355	274.026	3.08653	2.3467	11.088	191.276

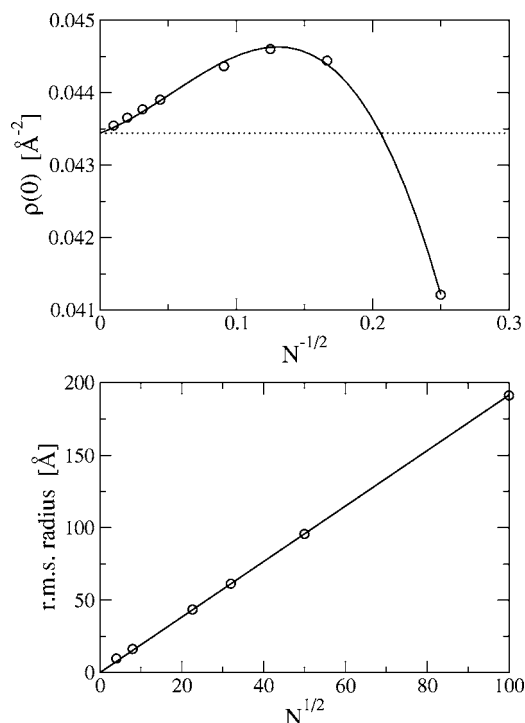


FIG. 6. (Top) Central density of  ${}^4\text{He}$  droplets as a function of  $N^{-1/2}$ . The empty circles correspond to the results obtained with the zero-range density functional, while the line stands for a cubic spline fit to these data. The dotted horizontal line indicates the saturation density  $\rho_0$ . (Bottom) Mean square radius of  ${}^4\text{He}$  droplets as a function of  $N^{1/2}$ . The solid line is a linear fit to the data without independent term. The empty circles correspond to the results of the zero-range density functional.

The mean square radius is shown in the lower panel of Fig. 6 as a function of  $N^{1/2}$ . The expected linear behavior, associated to a constant average density,

$$\langle r^2 \rangle^{1/2} = \frac{1}{\sqrt{2\pi\rho_0}} N^{1/2}, \quad (18)$$

is rather apparent. The fit to the calculated values, from  $N = 16$  to  $N = 10\,000$ , provides a  $\rho_0 = 0.0434 \text{ \AA}^{-2}$  in very good agreement with the equilibrium density used to define the parameters of the density functional.

#### IV. CONCLUSIONS

We have constructed a density functional suitable to study nonhomogeneous two-dimensional  ${}^4\text{He}$  systems. First, we have considered two-dimensional slabs to study the energy per particle, the central density, radius, and density profiles as a function of the coverage. We have analytically shown that the extracted linear tension from a mass formula adapted to this type of geometry is consistent with the value of the linear tension of the semi-infinite system which was used to build the density functional. The thickness and the central density of the slabs approach from below the values corresponding to the semi-infinite system while the radius diverges.

We have also studied the energetics and structure of two-dimensional clusters. In particular, we have considered clusters with a very large number of atoms to study the behavior of the mass formula and to establish how the system approaches the bulk limit. The central density of the clusters when  $N \rightarrow \infty$  approaches the saturation density from above, and therefore the internal regions of the clusters are more compressed than the bulk system, while the external regions have densities which would correspond to negative pressures or even below the spinodal point for a uniform system.

The profiles of the clusters are very well fitted by a generalized Fermi function. The thickness of the cluster slowly approaches the thickness of the semi-infinite system, as it also happens in the case of the slab geometries, but in this case from above. Finally, we have analyzed the linear behavior of the rms radius of the droplets in terms of  $N^{1/2}$ , and recovered the saturation density from the slope of this fit. The proposed density functional can be used with a very small computational effort for large clusters where the value of  $N$  is prohibitive for a Monte Carlo calculation.

#### ACKNOWLEDGMENTS

This work has been supported by DGICYT (Spain) Contract Nos. BFM2002-01868, PB2002-00200, and FIS2004-00912, by the Generalitat de Catalunya Project No. 2001SGR00064, and by the Junta de Andalucia. J.M.P. acknowledges financial support from the Generalitat de Catalunya.

<sup>1</sup>See, e.g., *Microscopic Approaches to Quantum Liquids in Confined Geometries*, edited by E. Krotscheck and J. Navarro Series on Advances in Quantum Many-Body Theories, Vol. 4 (World Scientific, Singapore 2002).

<sup>2</sup>M. Bretz, J. G. Dash, D. C. Hickernell, E. O. McLean, and O. E. Vilches, *Phys. Rev. A* **8**, 1589 (1973).

<sup>3</sup>B. E. Clements, J. L. Epstein, E. Krotscheck, and M. Saarela, *Phys. Rev. B* **48**, 7450 (1993).

<sup>4</sup>C. E. Campbell and M. Schick, *Phys. Rev. A* **3**, 691 (1971).

<sup>5</sup>P. A. Whitlock, G. V. Chester, and M. H. Kalos, *Phys. Rev. B* **38**, 2418 (1988).

<sup>6</sup>S. Giorgini, J. Boronat, and J. Casulleras, *Phys. Rev. B* **54**, 6099 (1996).

<sup>7</sup>B. Krishnamachari and G. V. Chester, *Phys. Rev. B* **59**, 8852 (1999).

<sup>8</sup>A. Sarsa, J. Mur-Petit, A. Polls, and J. Navarro, *Phys. Rev. B* **68**, 224514 (2003).

<sup>9</sup>S. Stringari and J. Treiner, *J. Chem. Phys.* **87**, 5021 (1987).

<sup>10</sup>M. Barranco, D. M. Jezek, E. S. Hernández, J. Navarro, and Ll. Serra, *Z. Phys. D: At., Mol. Clusters* **28**, 257 (1993).

<sup>11</sup>P. Hohenberg and W. Kohn, *Phys. Rev.* **136**, B864 (1964); W. Kohn and J. L. Sham, *ibid.* **140**, A1133 (1965); N. D. Lang and

- W. Kohn, Phys. Rev. B **1**, 4555 (1970).
- <sup>12</sup>F. Dalfovo, A. Lastri, L. Pricauenko, S. Stringari, and J. Treiner, Phys. Rev. B **52**, 1193 (1995).
- <sup>13</sup>S. Stringari, Phys. Lett. **107A**, 36 (1985).
- <sup>14</sup>C. Ebner and W. F. Saam, Phys. Rev. B **12**, 923 (1975).
- <sup>15</sup>S. Stringari and J. Treiner, Phys. Rev. B **36**, 8369 (1987).
- <sup>16</sup>L. Szybisz, Eur. Phys. J. B **14**, 733 (2000).
- <sup>17</sup>K. T. R. Davies, H. Flocard, S. Krieger, and M. S. Davies, Nucl. Phys. A **342**, 111 (1980).